U.D.C. 543.42;661.865.4

Advances in Electronic Raman Spectroscopy of the Lanthanides†

J.A.Koningstein

CONTENTS

I.	Introduction	834
II.	Vibrational and electronic Raman scattering	835
III.	The Raman scattering tensor	837
IV.	Intensity of Raman scattering and the crystal field	838
V.	The breakdown of selection rules	842
VI.	Experimental methods	843
VII.	Experimental results	845

I. INTRODUCTION

Since the discovery of Raman scattering (RS), many investigators based their explanation of the characteristics of the spectra of solids, liquids, and gases on Placzek's work. Despite the fact that the first studies on Raman scattering were carried out by physicists, during the period from 1935 until the introduction of the laser, this type of spectroscopy has been used extensively by chemists as a means of establishing molecular structures. The vibrational and rotational Raman spectra have been almost always excited by a low-pressure mercury lamp which precluded a direct comparison of specific experimental data with theory. For example, it was difficult to obtain information about the individual elements of the scattering tensor, since the direction of propagation of the exciting radiation was not exactly parallel or perpendicular to the direction of the observation of the scattered radiation. The measured degrees of depolarisation of the Raman lines of liquids and gases almost always differed from the theoretical values, so that the calculation of the degrees of depolarisation of vibrations of a particular type or the *a priori* calculation of absolute intensities constituted a cumbersome procedure.

Most of the experimental studies during the above period dealt with the excitation of Raman transitions in the vibrational or rotational molecular levels. All these levels are linked to the electronic ground state of the molecule. Electronic Raman scattering was observed only for the NO molecule[1]. In 1932 Rasetti attributed the 121 cm^{-1} Raman line for this molecule to the $^2\Pi_{1/2}-{}^2\Pi_{3/2}$ transition. According to Gerding's evidence, Gorter undertook experiments with lanthanide ions during the second world war and it was not until 1964 that Hougen and Singh[3] succeeded in exciting Raman scattering in the electronic transitions of Pr^{3+} in $PrCl_3$. Immediately before the publication of this paper, Elliott and Loudon[4] predicted the possibility of observing electronic Raman scattering by lanthanide ions. In addition, Chau observed Raman scattering for Ce^{3+} in $CaWO_4$.[5] In all the experiments the mercury lamp still served as the light source and photographic plates were used to record the spectra. Very little information was obtained about the intensity of this effect relative to the intensities of strong Raman lines for certain well known liquids.

† This is an English translation of the review published by the author in Russian (Ed. of Translation).

Placzek pointed out that the scattering tensor for electronic transitions differs from the scattering tensor for vibrational and rotational transitions[6,9]. In the latter case the tensor is symmetric, whereas the tensor for electronic transitions may become antisymmetric.

Numerous crystalline compounds containing lanthanide ions are now available and, when it is necessary to separate the phonon Raman spectrum from electronic effects, the elements of the scattering tensor must be investigated.

In 1966 the author of the present review began a programme devoted to the excitation of electronic Raman scattering of lanthanide ions in certain crystals using the radiation from a helium–neon laser at 6328 Å. By that time it became clear that the individual elements of the Raman scattering tensor for vibrational transitions can be measured and there was hope that measurements of this type might be carried out also for electronic transitions. The helium–neon laser was chosen because, as can be seen from the energy level diagram for lanthanide ions, only a few of them have excited states with energies equal to those of the laser emission (Fig. 1). By employing a more sensitive recording system, the author succeeded in 1966 in exciting the Raman spectra of tervalent lanthanide ions in the lattice of the yttrium–gallium garnet[6,7]; this was followed by a series of experiments on the same ions in other crystals[8-12].

In Placzek's theory of polarisability for vibrational Raman scattering, attention was concentrated on the polarisability of the molecular ground state and the role of the intermediate states was to a considerable degree limited. The matrix elements of the electrical dipole moment operator for transitions between the ground and intermediate states appear in the expressions for the elements of the scattering tensor. In the general case, our knowledge of the wave functions for these states is insufficient to calculate the matrix elements and hence we have also to calculate the elements of the scattering tensor for vibrational transitions. The situation is almost completely different for tervalent lanthanide ions. The wave functions for the states of the lanthanide ions—free or in an environment of specified symmetry—have been calculated and Axe[13] used these wave functions in the calculation of the absolute Raman intensities in the electronic transitions of certain lanthanide ions. In these calculations the effect of the antisymmetry of the scattering tensor was neglected.

However, Mortensen and the present author[14] showed that a large contribution by antisymmetric tensors to the total intensities may be expected from many ions. Indeed,

in certain cases the contribution from antisymmetric tensors is greater than that from symmetrical tensors and at least one case has been found where the Raman transitions are due to a completely antisymmetric tensor[9]. Apart from the absolute intensities, the ratio of the intensity of Rayleigh scattering to the intensity of electronic Raman scattering of all the lanthanides has also been calculated[15] and in subsequent reports a relation was established between the force and symmetry of the crystal field on the one hand and the polarisation characteristics of the complete electronic Raman spectra on the other[16,17].

Following the appearance of the argon and krypton ionic lasers towards the end of 1970, more detailed experimental data were obtained[18] and electronic Raman scattering was observed for all lanthanide ions with two exceptions[19,20]. The experimental results confirmed the theoretical prediction that the intensity of the electronic Raman lines is lower than the intensity of scattering by the crystal matrix phonons. It was also noted that the intensities depend greatly on the electronic configuration of the ions. However, the contribution of antisymmetric tensors to the intensity is less marked, with the exception of the Eu^{3+} ion, where the scattering is entirely due to the antisymmetric tensor[21]. The appearance of this tensor is unique in physics and chemistry and in Raman spectroscopy is a result of profound changes in selection rules.

A glance at the energy level diagrams (Fig. 1) shows that many levels have been designated by the quantum number J which is a multiple of 1/2. This implies that representations of binary groups must be used for the investigation of the symmetry of the levels in the crystal field and of the scattering tensor components. The main result is that the tensors for electronic and vibrational transitions are completely different in all the crystals[22].

We shall conclude the introduction with general remarks concerning the selection rules for Raman scattering[23]. All the states arising from the same electronic configuration have the same parity—they are either even or odd. The scattering operator $\hat{\alpha}_{\rho\sigma}$ (where ρ and $\sigma = x, y, z$) is an even operator and the integral $\int \Psi_n \hat{\alpha}_{\rho\sigma} \Psi_m d\tau \neq 0$, where Ψ_n and Ψ_m are the wave functions of these states. Thus, like vibrational and rotational scattering, electronic scattering is formally allowed.

II. VIBRATIONAL AND ELECTRONIC RAMAN SCATTERING[14,15]

We shall suppose that a photon flux is incident on atoms, molecules, or a crystal. Most of these photons will not interact with the species but some of them (less than 1%) will be involved in an elastic interaction. The frequency of the electromagnetic radiation then remains unchanged and the elastic interaction leads to the so-called Rayleigh scattering. However, a much smaller number of protons are scattered inelastically. An atom, ion, or molecule may be excited from the ground to the first or second excited state and, when this has happened, the law of conservation of energy shows directly that the scattered photons have an energy and consequently a frequency differing somewhat from that of the incident photons. It is of course also possible that a species can return from the excited to the ground state, whereupon the [liberated] energy is added to the energy of the incident photons, which leads to a decrease of the wavelength of the scattered radiation. Thus the Raman spectrum appears in the form of emission lines corresponding to greater and smaller energies than the undisplaced Rayleigh scattering lines. Since in the excited states there are fewer species than in the ground state, the intensity of the so called anti-Stokes Raman lines is lower than of the Stokes Raman lines. The intensity ratio of these lines is specified by the Boltzmann distribution law. However, in order to obtain a clear description of the Raman intensity, it is necessary to examine this process in greater detail.

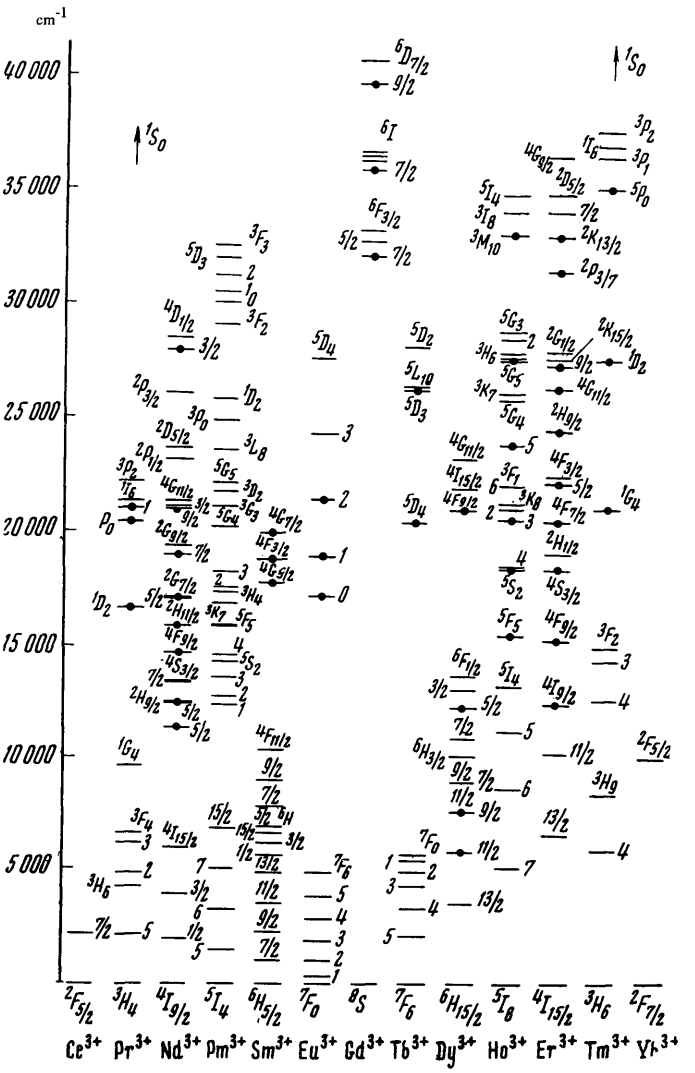


Figure 1. Energy level diagrams for tervalent lanthanide ions. The emission energy of the He—Ne and Ar^+ lasers is between 15 000 and 22 000 cm^{-1}. Certain lanthanide ions absorb this radiation with a consequent appearance of fluorescence, which precludes the observation of electronic Raman scattering.

Fig. 2 represents the case where the incident radiation is propagated along one of the axes of the rectangular coordinate system and the scattered radiation is observed in

the direction perpendicular to that of the propagation of the incident light rays. We shall suppose that at the origin of the rectangular coordinate system there is a single crystal with cubic symmetry and that its macroscopic axes coincide with the x, y, and z axes of the coordinate system. The electric field of the incident wave may induce a dipole moment in the atom or molecule of the crystal. In the general case, the direction of this induced moment will not be parallel to the electric vector of the incident wave. Raman scattering may be described by the tensor

$$\mu^i = (\alpha)\, E,$$

where

$$\begin{aligned} \mu_x^i &= \alpha_{xx}E_x + \alpha_{xy}E_y + \alpha_{xz}E_z, \\ \mu_y^i &= \alpha_{yx}E_x + \alpha_{yy}E_y + \alpha_{yz}E_z, \\ \mu_z^i &= \alpha_{zx}E_x + \alpha_{zy}E_y + \alpha_{zz}E_z. \end{aligned} \qquad (1)$$

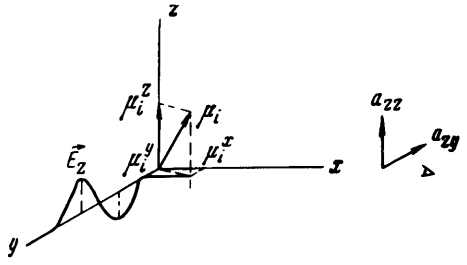


Figure 2. Raman scattering in a cubic crystal the a, b, and c axes of which are parallel to the axes of the cartesian coordinate system. The laser radiation enters the crystal in the direction of the y axis and the scattered Raman radiation is observed along the x axis. The induced dipole moment μ_i and its components μ_i^z, μ_i^y, and μ_i^x are shown. By placing an analyser in front of the monochromator, it is possible to resolve the α_{zz} and α_{zy} components. They appear in the $y(zz)x$ and $y(zy)x$ polarisation Raman spectra.

In each specific case different components of the scattering tensor can be determined by a suitable choice of direction of the polarisation of the incident radiation, the crystal orientation, and the direction of observation of the scattered radiation. Hitherto, we have not discussed the types of Raman scattering. Raman spectroscopy has proved to be a very successful method for the determination of molecular structures in the gas phase, in liquids, and crystals using rotational or vibrational spectra.

The induced moment for vibrational Raman scattering is the transition moment between the ground and excited vibrational states. In order to relate the intensity of the Raman line to the elements of the scattering tensor, the polarisability of the molecule in the ground state $(\alpha_{\rho\sigma})$ is formulated in the form of an expansion in terms of the coordinates of the normal vibrations of the molecule. The intensity of the Raman lines is related to the derivatives of the polarisability[24] of the molecule in the ground state with respect to the normal coordinates (Q). Recently another model was proposed[25] for vibrational Raman scattering. The following expression, obtained for the components of the scattering tensor $(\alpha_{\rho\sigma})_{kn}$ (where ρ and $\sigma = x, y, z$), was used for the transition between the states k and n of the system:

$$(\alpha_{\rho\sigma})_{kn} = h^{-1}\sum_r \frac{\langle n|e\sigma|r\rangle\langle r|e\rho|k\rangle}{\nu_0 - \nu_{kn}} + \frac{[\rho \leftrightarrow \sigma]}{\nu_0 + \nu_{kn}}. \qquad (2)$$

The subscripts k and n in Eqn. (2) show that Raman scattering begins from the state k and terminates at the state n, ν_0 is the frequency of the incident light, $\langle n|e\sigma|r\rangle$ is a matrix element of the electric dipole moment, and the summation with respect to r is carried out over all the excited states of the system. The electric dipole moment can be formulated as follows:

$$\int \Psi_n^* e\sigma \Psi_r d\tau.$$

In the general case, the wave function Ψ_n is defined as the product of the electronic wave function $\Psi_n(\mathbf{r}Q)$ and the vibrational wave function $\varphi_v(Q)$, where n is the electronic quantum number, v the vibrational quantum number, and Q the normal coordinate. The electronic motions may be sensitive to the motions of the nuclei in the molecule. Assuming that this interaction is weak, the following form may be used for the Hamiltonian $\mathcal{H}$:

$$\mathcal{H} = \mathcal{H}_0 + \left(\frac{\partial \mathcal{H}}{\partial Q}\right)_{Q=0} Q + \ldots$$

and the wave function

$$\begin{aligned} \Psi_n(\mathbf{r}, Q) &= \Psi_n^0(\mathbf{r}, Q=0) + \\ &+ \sum_{l\neq n} \frac{\int \Psi_l^0(\mathbf{r}, Q=0)\left(\frac{\partial \mathcal{H}}{\partial Q}\right)_{Q=0} \Psi_n^0(\mathbf{r}, Q=0)\, Q d\tau}{E_l^0 - E_n^0} \Psi_l^0(\mathbf{r}, Q=0), \end{aligned} \qquad (3)$$

where $\mathcal{H}_0$ is the Hamiltonian of the vibrating molecule in the equilibrium configuration and E_l^0 is the energy of the first excited electronic state of the molecule.

The electronic wave functions in the form of a series [Eqn. (3)] can now be substituted in the expression for the matrix elements of the electric dipole moment, which enters into the component of the scattering tensor in Eqn. (1). Fortunately, it is possible to make certain simplifications and to obtain the following relations.

I. Electronic Raman scattering (n; $v = 0 \rightarrow k$; $v = 0$):

$$(\alpha_{\rho\sigma})_{nv=0;kv=0} = h^{-1}\sum_r \left\{\frac{(M_\rho)_{nr}(M_\sigma)_{rk}}{\nu_{rk} - \nu_0} + \frac{[\rho \rightarrow \sigma]}{\nu_{rn} + \nu_0}\right\}. \qquad (4a)$$

II. Vibronic Raman scattering (n; $v \rightarrow k$; v'):

$$(\alpha_{\rho\sigma})_{nv;kv'} = h^{-1}\langle\varphi_{v'}|Q|\varphi_v\rangle \sum_r \left\{\frac{(M_\rho)_{kr}[(M_\sigma)_{rl}h_{ln}^Q + (M_\rho)_{ln}h_{lr}^{Q*}]}{\nu_{rk} - \nu_0} + \ldots\right\}. \qquad (4b)$$

The constant h_{ln}^Q is defined by the integral

$$\int \Psi_l^0(\mathbf{r}, Q=0)\,(\partial\mathcal{H}/\partial Q)_{Q=0}\Psi_n^0(\mathbf{r}, Q=0)\, d\tau/(E_l^0 - E_n^0).$$

If the vibronic interaction is weak, it follows automatically that the constants h_{ln}^Q are small. As a result, we find that the main contribution to the intensity of electronic Raman scattering levels comes from the elements of the scattering tensor $(\alpha_{\rho\sigma})_n$; $v = 0 \rightarrow k$; $v = 0$. Vibronic Raman scattering is probably insignificant compared with the more intense electronic Raman scattering in the transition between the states k and n.

It is interesting to replace the quantum number n by k in Eqns. (4a) and (4b). The first of these equations becomes identical with the expression for Rayleigh light

scattering. The replacement of n by k in Eqn. (4b) leads to the relation

$$(\alpha_{\rho\sigma})_{v;v'} = \hbar^{-1}\langle\varphi_{v'}|Q|\varphi_v\rangle \sum_r \left\{\frac{(M_\rho)_{nr}[(M_\sigma)_{rl}h^Q_{ln} + (M_\rho)_{ln}h^{*Q}_{lr}]}{\nu_{rn}-\nu_0} + \ldots\right\}, \quad (5)$$

which gives the elements of the Raman scattering tensor for the transition between the vibrational levels v and v' linked to the same ground electronic state n. Thus vibrational Raman scattering has now been described in terms of a model where interaction with vibrations has been introduced. This model, incorporating vibronic interactions, was proposed, as already stated, by Albrecht[25], who also showed that the selection rules for Raman scattering may be obtained by examining the conditions under which the constants h^Q_{nl} and h^Q_{lk} are not zero.

Eqns. (4a) and (5) may be used directly to investigate the symmetry of the scattering tensor. The tensor is symmetric if the element $(\alpha_{\rho\sigma})_{nk}$ is equal to the element $(\alpha_{\sigma\rho})_{nk}$. For vibrational Raman scattering levels, the tensor is symmetric, but for electronic Raman scattering it is found that this condition is not obligatory. One should probably note here that the antisymmetry of the scattering tensor at vibrational levels can also obtain if (a) the wave function entering into the matrix elements of the electric dipole moment operator are not real or (b) the electronic ground state of the molecule is degenerate. The vibrational model loses validity for a degenerate ground state and the considerations employed to obtain expressions for a non-degenerate ground state are inapplicable in this instance.

The transition between the states k and n is allowed in Raman scattering if the matrix element $\langle k|\hat{\alpha}_{\rho\sigma}|n\rangle \neq 0$. The operator $\hat{\alpha}_{\rho\sigma}$ can be formulated as follows:

$$(\hat{\alpha}_{\rho\sigma})_{kn} = \sum_r \frac{|e\sigma|r\rangle\langle r|e\rho|}{\nu_0 - \nu_{kn}} + \frac{[\rho\to\sigma]}{\nu_0 + \nu_{kn}}. \quad (6)$$

In order to find the conditions under which the matrix element does not become zero, it is necessary to know the transformation properties of the wave functions of the states k and n and the symmetry properties of the scattering tensor itself. The matrix element does not become zero if the direct product of the irreducible representations of the wave functions of k and n and the tensor contains a fully symmetric representation of the point groups. The symmetry properties of the electronic levels may be obtained, for example, from crystal field calculations. The transformation properties of the elements of the scattering tensor are sometimes quoted in the tables of characters of various point groups. However, these data refer only to the special case of vibrational or rotational Raman scattering and above it was shown that in this case the tensor is symmetric. Thus the question arises of what changes occur in the transformation properties when the tensor becomes antisymmetric.

III. THE RAMAN SCATTERING TENSOR

The transformation properties of the antisymmetric part of the scattering tensor are specified by the symmetry of the $\alpha_{\rho\sigma} - \alpha_{\sigma\rho}$ ($\sigma, \rho = x, y, z$) combinations. The transformation properties of these combinations are not quoted directly in the tables of characters of various point groups. It can be shown that the antisymmetric combinations for all rotations transform as an ordinary vector, and in inversion the transformation is more as an axial vector than a polar vector. This is also valid for the transformation properties of the rotations about the axes of the cartesian coordinate system (R_Z, R_Y, and R_X), so that the transformation properties of the transformation of the antisymmetric part of the scattering tensor and of the rotations about R_Z, R_Y, and R_X are analogous. They can be found directly from the character tables, for example those quoted by Wilson et al.[26]

Ions in crystals occupy positions with specific symmetry. Thus the components of the tensor and the wave functions of the electronic levels may be designated in accordance with the representation of the known point groups. However, the angular components of the electronic wave functions are formulated in terms of the polar coordinates r, θ, and φ, while the symmetry of the tensor was considered above in terms of cartesian coordinates.

The intensity of Raman scattering in an electronic transition is proportional to the square of the matrix element $\langle n|\hat{\alpha}_{\rho\sigma}|m\rangle$, but the n and m wave functions of the operator $\hat{\alpha}_{\rho\sigma}$ have still not been defined in terms of the same coordinate system.

The tensor $(\alpha_{\rho\sigma})$ can be transformed into one in terms of spherical coordinates. These new tensors are irreducible and their components are designated by α^K_Q. The difference between the cartesian and irreducible tensors is that the components of the latter can be combined into three separate sets. In an arbitrary rotation, the members of each set are transformed into one another (or into their combinations), which does not happen for the components of the tensor in terms of cartesian coordinates. The relation between $\alpha_{\rho\sigma}$ and α^K_Q is indicated in Table 1.

Table 1. Relation between the components of the tensor in the cartesian coordinate system and the components of irreducible tensors.

$\alpha^0_0 = -(1/\sqrt{3})(\alpha_{xx}+\alpha_{yy}+\alpha_{zz})$,	$\alpha^2_2 = \frac{1}{2}(\alpha_{xx}-\alpha_{yy}+i\alpha_{xy}+i\alpha_{yx})$,
$\alpha^1_1 = \frac{1}{2}(-\alpha_{xz}+\alpha_{zx}-i\alpha_{yz}+i\alpha_{zy})$,	$\alpha^2_1 = -\frac{1}{1}(\alpha_{xz}+\alpha_{zx}+i\alpha_{yz}+i\alpha_{zy})$,
$\alpha^1_0 = (1/\sqrt{2})(i\alpha_{xy}-i\alpha_{yx})$,	$\alpha^2_0 = (1/\sqrt{6})(2\alpha_{zz}-\alpha_{xx}-\alpha_{yy})$,
$\alpha^1_{-1} = -\frac{1}{2}(\alpha_{xz}-\alpha_{zx}-i\alpha_{yz}+i\alpha_{zy})$,	$\alpha^2_{-1} = \frac{1}{2}(\alpha_{xz}+\alpha_{zx}-i\alpha_{yz}-i\alpha_{zy})$,
	$\alpha^2_{-2} = \frac{1}{2}(\alpha_{xx}-\alpha_{yy}-i\alpha_{xy}-i\alpha_{yx})$.

It is useful to compare the three sets of irreducible tensor components and the s, p, and d orbitals defined in terms of polar coordinates. Like the s orbitals, the irreducible tensor component α^0_0 is completely invariant for all rotations, while the $\alpha^1_{1,0,-1}$ components are mainly transformed like the p orbitals: p_X, p_Y, and p_Z. However, there is a small difference: the orbitals change sign following the inversion of the coordinate system, while the tensor components are invariant in this operation. There is also an analogy between the transformation properties of the d orbitals and the five α^2_Q components ($Q = 2, 1, 0, -1, -2$).

Suppose, for example, that an electronic Raman transition has been induced between the states ^1S and ^3P with the electronic configuration $(p)^2$. We assume that an atom or ion is located in the crystal in a position where

the symmetry is very high, for example O_h. A necessary condition for the Raman scattering in the electronic transition to be allowed is that the fully symmetric representation of the point group is contained in the direct product of the representations:

$$\Gamma_i \times \Gamma_{\alpha_Q^K} \times \Gamma_i .$$

The state (i), which is the lowest in Raman scattering, transforms as the fully symmetric representation of the point group and it is therefore seen that the non-zero components of the scattering tensor transform as the representation to which the finite state p belongs. This finite state is a spectroscopic P state ($l = 1$) and the non-zero components of the scattering tensor α_Q^K are those which transform as the p orbitals. The α_Q^1 components constitute the antisymmetric part of the scattering tensor (see Table 1); Raman scattering in the transition between these states is related to the scattering tensor, which is partly asymmetric. The components of the irreducible tensors may be used not only to establish the selection rules but also they are important for the calculation of the absolute Raman intensities.

In translational Raman scattering, such calculation is very difficult, since in the expression for the tensor element [Eqn. (1)] it is necessary to carry out a summation over all the states r of the system. For electronic Raman scattering, these states are purely electronic and not vibrational, which simplifies the calculations. If the average frequency $\tilde{\nu}_{\chi k}$ is determined by the centre of gravity of the energy $h\tilde{\nu}_{\chi k}$ of one specific excited configuration, the denominator in Eqn. (1) becomes

$$(\nu_{kr} - \nu_0)^{-1} = (\tilde{\nu}_{\chi k} - \nu_0)^{-1}(1 + x + x^2 + \ldots), \qquad (7)$$

where

$$x = (\tilde{\nu}_{\chi k} - \nu_{rk})/(\tilde{\nu}_{\chi k} - \nu_0).$$

The $4f-5d$ transition in Ce^{3+} has a frequency of about 50 000 cm^{-1}. If the Raman spectra are excited by light with a frequency $\nu_0 = 20\,000$ cm^{-1}, then $x > 1$, since all the states r have almost the same energy. Moreover, the frequency dependence of the summation is now found from the terms ν_{rk}, where r are the states of an individual electronic configuration.

We now have

$$\langle r|[\mathcal{H}\sigma]|k\rangle = \langle \mathcal{H}r|\sigma|k\rangle - \langle r|\sigma\mathcal{H}|k\rangle = (\nu_{rk}/h)\langle r|\sigma|k\rangle \quad , \qquad (8)$$

where $\mathcal{H}$ is the Hamiltonian of the system and σ is the electric dipole moment of the operator. Combination of Eqns. (7) and (8) with Eqn. (4a) yields

$$(\alpha_{\rho\sigma})_{kn} \approx \sum_r \frac{1}{h}\frac{\tilde{\nu}_{\chi k}\langle n|\rho|r\rangle\langle r|[\mathcal{H}\sigma]|k\rangle}{\tilde{\nu}_{\chi k} - \nu_0} + \frac{\tilde{\nu}_{\chi n}\langle n|[\mathcal{H}\sigma]|r\rangle\langle r|\rho|k\rangle}{\tilde{\nu}_{\chi n} + \nu_0} . \qquad (9)$$

If the Raman intensity is now specified by the integral $\langle k|\hat{\alpha}_{\rho\sigma}|n\rangle$ then the operator $\hat{\alpha}_{\rho\sigma}$ becomes

$$\hat{\alpha}_{\rho\sigma} \simeq \sum_r \frac{\tilde{\nu}_{\chi k}\{|\rho|r\rangle\langle r|[\mathcal{H}\sigma]|\}}{\tilde{\nu}_{\chi k} - \nu_0} + \frac{\nu_{\chi n}\{|[\mathcal{H}\sigma]r\rangle\langle r|\rho|\}}{\tilde{\nu}_{\chi n} + \nu_0} . \qquad (10)$$

The wave functions $|r\rangle$ and $|n\rangle$ of tervalent ions are in the general case characterised by the quantum numbers $nLSJJ_Z$. Under the influence of the crystal field, the LSJ sets split into $2J + 1$ components, as a result of which the states of the crystal field are no longer pure J_Z substates but represent a mixture of J_Z substates resembling that formulated below:

$$|\Psi\rangle = a_{nLSJJ_z}|J, J_z\rangle + a_{nLSJJ'_z}|J, J'_z\rangle + \ldots + a_{nLSJ-J_z}|J, -J_z\rangle \qquad (11)$$

$$\rangle \sum_{J_z} a^2_{nLSJJ_z} = 1.$$

If the coefficients a are introduced into Eqns. (9) or (10), then the single summation with respect to the states r assumes the following form:

$$\sum_{nLSJJ_z}\sum_{nLSJJ'_z}\sum_{n''L''S''J''J''_z} a(nLSJJ_z)\, a(nLSJJ'_z)\, a(n''L''S''J''J''_z) , \qquad (12)$$

where all the wave functions have been normalised. Consequently, similarly to Eqn. (11), we have

$$\sum_{J_z \in \chi} a^2(n'L''S''J''J''_z) = 1. \qquad (13)$$

We can now introduce the components of the irreducible tensors and employ Judd's sums rule, since two operators $\hat{\rho}$ and $[\mathcal{H}\sigma]$ appear in the operator $\hat{\alpha}_{\rho\sigma}$ [Eqn. (10)]. We obtain the following final expression for the element α_Q^K:

$$\hat{\alpha}^{'K}_{knp} = \sum_{\nu SLJM}\sum_{\nu' SL'J'M'} a^*(n;\gamma'SL'J'M')\, a(k;\gamma SLM)\langle\gamma'SL'J'M'|U^K_Q|\gamma SLJM\rangle + \\ + \sum_{\chi}\left[\sum_{i=0}^{p}\binom{p}{i}\left(-\frac{1}{h}\right)^i\left\{\frac{(\bar{\nu}_{\chi k})^{p-i}}{(\bar{\nu}_{\chi k} - \nu)^{p+1}}(nl\|r\|n'l')(n'l'\|[\mathcal{H}^i r]\|nl)\times\right.\right. \\ \left.\left.\times(-1)^i\frac{(\bar{\nu}_{\chi n})^{p-i}}{(\bar{\nu}_{\chi n} + \nu)^{p+1}}(-1)^K(nl\|[\mathcal{H}^i r]\|n'l')(n'l'\|r\|nl)\right\}\right]\times \\ \times(2K+1)^{1/2}\begin{Bmatrix} 1 & K & 1 \\ l & l' & l\end{Bmatrix}(-1)^K \qquad (14)$$

and for the matrix element

$$\langle\gamma'SL'J'M'|U^K_Q|\gamma SLJM\rangle = (-1)^{J'-M'}\begin{pmatrix} J' & K & J \\ -M' & Q & M\end{pmatrix}\times \\ \times\langle\gamma'SL'J'\|U^K\|\gamma SLJ\rangle \quad . \qquad (15)$$

Raman scattering has now been formulated for transitions between the crystal field states $|SLJJ_Z\rangle$ and $|SL'J'J'_Z\rangle$; here

$$(nl|r|n'l') = \int R_{nl}(r)\, R_{n'l'}\, d\tau \quad .$$

$|n'l'\rangle$ are wave functions for the excited configuration. The values of the matrix elements $\langle n'SL'\|U^K\|nSL\rangle$ have been published by Nielson and Koster[27].

One can gain a better understanding of the essential feature of the selection rules for Raman scattering from the knowledge of the conditions under which the j-symbol is non-zero:

$$\begin{pmatrix} J' & K & J \\ -J'_z & Q & J_z\end{pmatrix} \quad . \qquad (16)$$

The $3j$-symbol is automatically zero if $-J'_Z + Q + J_Z$ and $J' + K + J$ do not simultaneously satisfy the usual triangle conditions (for $J = 0$, this implies that $J' = K$). The selection rules with respect to J are $\Delta J \leq 2$ and also $\Delta S = 0$ and $\Delta L \leq 2$. Thus the additional conditions in the calculation of the scattering tensor are as follows: (a) expansion (7) must be valid and (b) all the states involved in Raman scattering must be those of the crystal field and not the ligand field.

IV. INTENSITY OF RAMAN SCATTERING AND THE CRYSTAL FIELD

Having an expression for α_Q^K, it is possible to calculate the ratios $\alpha_0^0/(\alpha_Q^1 + \alpha_Q^2)$ and α_Q^1/α_Q^2. The first represents the ratio of the intensities of Rayleigh and Raman scattering and the second the ratio of the antisymmetric and symmetrical parts of the Raman scattering tensor. Fig. 3 presents the Rayleigh and Raman intensity ratios for all the lanthanides where there is a transition between

the lowest and subsequent manifold LSJ states of the free ions. These manifold states for Ce, Pr, Nd, Sm, Eu, Tb, and Dy have an energy greater by 2500 cm^{-1} than that of the ground state, while for Tm and Yb the energy is greater by 10000 cm^{-1}. In the general case, the ratio is between 10^2 and 10^3, i.e. approximately the same as for Raman scattering in vibrational transitions.

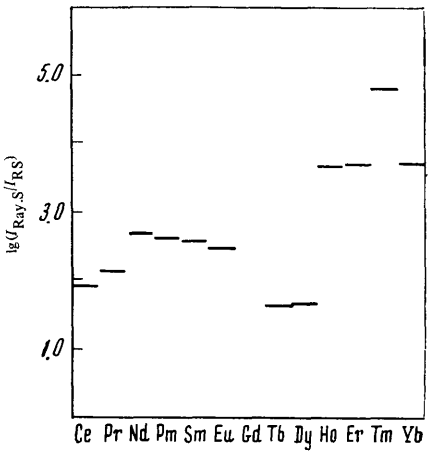


Figure 3. The ratio of the Rayleigh and electronic Raman scattering intensities of tervalent lanthanide ions. The Raman scattering takes place between the set of levels of the ground state and the first higher set of levels. For Yb^{3+}, the difference between the energies of these levels is about 10000 cm^{-1}, which accounts for the higher Rayleigh and Raman intensity ratio, since the intensity of the Raman lines (Stokes lines) is proportional to $(\nu_0 - \nu_{kn})^4$.

Table 2 lists the scattering cross-sections for certain electronic effects. The absolute value of 10^{-32} cm^2 for electronic scattering may be compared with 10^{-28} cm^2 [the experimental value for the $\nu_1(C_6H_6)$ line at 992 cm^{-1}] for vibrational Raman scattering[28]. Thus the intensity of the electronic transitions is lower than that of the majority of the vibrational Raman bands. The fact that one cannot neglect the antisymmetry of the scattering tensor becomes evident when the theoretical results in Fig. 4 are compared. The degree of antisymmetry diminishes if the transition is between states with different values of J; however, lanthanide ions with less than seven f electrons show a higher degree of antisymmetry. It was shown in Section III that the transition associated with the $\alpha_{\rho\sigma} - \alpha_{\sigma\rho}$ ($\alpha_Q{}^1S$) tensor combination is possible only for electronic Raman scattering.

Table 2. Absolute cross-sections[a] of Rayleigh and electronic Raman scattering of Pr^{3+} and Tm^{3+} ions.

Ions	Rayleigh scattering, cm^2	Raman scattering	Transition in Raman scattering
Pr^{3+}	$0.9\cdot10^{-29}$	$0.6\cdot10^{-31}$	$^3H_4 \rightarrow {}^3H_5$
Tm^{3+}	$1.3\cdot10^{-30}$	$0.2\cdot10^{-39}$	$^3H_6 \rightarrow {}^3H_4$

[a]The calculation was made for exciting radiation at a wavelength of 6328 Å.[15]

The relation between the transitions in electronic Raman scattering and the symmetry of the crystal field, which is shown for ions in solids, is also specified by Eqn. (14). The linear combination of the substates J_Z, which are the wave functions of the crystal field levels [Eqn. (10)], is in fact determined by the crystal field symmetry and the strength and symmetry of the field appear in the expressions for the mixing coefficients a.

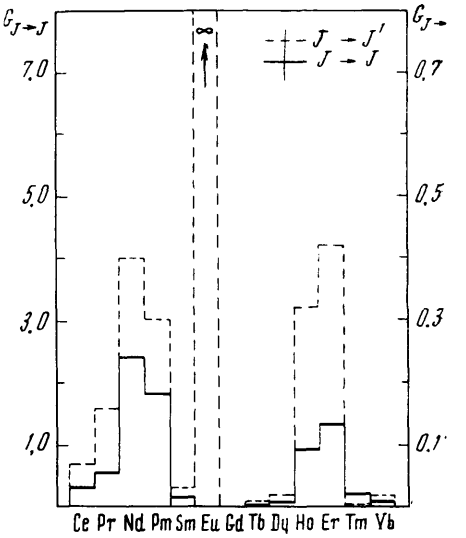


Figure 4. The calculated degree of antisymmetry of the tensor for electronic Raman scattering of tervalent lanthanide ions.

These coefficients and therefore the correct wave functions may be found by diagonalising the matrix comprising the elements $\langle J, J_Z | H_{CF} | J', J'_Z \rangle$, where H_{CF} denotes the effective potential due to neighbouring ions at the site of the jth electron of the lanthanide ion located in the centre. H_{CF} can be expressed in the following form:

$$H_{CF} = -e\sum_j V(r_j, Q_j, \varphi_j) \quad . \tag{17}$$

In the calculation of the crystal field, the perturbation Hamiltonian is usually formulated thus:

$$\mathcal{H}_{CF} = \sum_n \sum_{m=-n}^{n} \sum_j B_n^m r_j^m Y_j^m(\theta_j, \varphi_j) \quad . \tag{18}$$

The B_n^m are constants and their values are in principle determined by the positions and charges of the ions surrounding the lanthanide ions, r_j is the expectation radius of the jth $4f$ electron, and Y_n^m are spherical harmonics. The expansion for f electrons should include terms up to $n \leq 6$ subject to the condition $n \leq 2J$.

The eigenvectors, eigenvalues, the values of α_Q^K, and the elements of the tensor in terms of cartesian coordinates for the tervalent europium ion in a crystal field with tetragonal symmetry, determined by the parameters B_2^0, B_4^0, B_4^4, and B_6^0, are given in Table 3. Figs. 5, 6, and 7 illustrate the calculated polarised spectra of this ion in certain crystal fields.

The electronic transitions in Raman scattering are $^7F_0 \rightarrow {}^7F_1$ (<600 cm^{-1}) and $^7F_0 \rightarrow {}^7F_2$ (>600 cm^{-1}). All the

tensors for the transitions $J = 0 \rightarrow J = 1$ are fully antisymmetric and all the tensors for the transitions $J = 0 \rightarrow J = 2$ are fully symmetric. Such tensors may be separated from one another by the rotation of the entire crystal about the fourfold axis; the differences in Raman intensity under the conditions of the observation of $z(xy)x$ for the symmetrical tensor and the fully antisymmetric tensor are presented in Fig. 8. Table 3 shows that the coefficients a are completely independent of the crystal field parameters and consequently the number of Raman lines in the spectra obtained for different polarisations is the same for all the crystal fields with tetragonal symmetry, but the frequency of the Raman lines depends in all cases on the parameters B_n^m.

Table 3. The eigenvalues, eigenvectors, and scattering tensors for the Eu^{3+} ion in a tetragonal crystal field[a,b].

Eigenvalue	Eigenvector	Controlling element α_Q^K	$\alpha_Q^K/F(K,\nu)$	Scattering tensor
		$^7F_0 \rightarrow {}^7F_2$		
$2\alpha A_2 + \beta(A_4^0 - A_4^4)$	$(1/\sqrt{2})(\lvert 2,2\rangle - \lvert 2,-2\rangle)$	α_{-2}^2	$+(1/70)^{1/2}$	$\alpha_{-2}^2\begin{bmatrix} 1/2 & -i/2 & 0 \\ -i/2 & -1/2 & 0 \\ 0 & 0 & 0 \end{bmatrix}$
$2\alpha A_2^0 + \beta(A_4^0 + A_4^4)$	$1/\sqrt{2}(\lvert 2,2\rangle - \lvert 2,-2\rangle)$	α_2^2	$+(1/70)^{2/3}$	$\alpha_2^2\begin{bmatrix} +1/2 & -i/2 & 0 \\ -i/2 & -i/2 & 0 \\ 0 & 0 & 0 \end{bmatrix}$
$-\alpha A_2^0 + 4\beta A_4^0$	$1(\lvert 2,1\rangle \lvert)$	α_1^2	$-(1/35)^{1/2}$	$\begin{bmatrix} 0 & 0 & -1/2 \\ 0 & 0 & -i/2 \\ -1/2 & -i/2 & 0 \end{bmatrix}$
$-\alpha A_2^0 - 4\beta A_4^0$	$1(\lvert 2,-1\rangle \lvert)$	α_{-1}^2	$+(1/35)$	$\alpha_{-1}^2\begin{bmatrix} 0 & 0 & -1/2 \\ 0 & 0 & -i/2 \\ -1/2 & -i/2 & 0 \end{bmatrix}$
$-2\alpha A_2^0 + 6\beta A_4^0$	$1(2,0\rangle)$	α_0^2	$-(1/35)$	$\alpha_0^1\begin{bmatrix} -2/\sqrt{6} & 0 & 0 \\ 0 & -1/\sqrt{6} & 0 \\ 0 & 0 & 2/\sqrt{6} \end{bmatrix}$
		$^7F_0 \rightarrow {}^7F_1$		
$-2\alpha A_2^0$	$1(\lvert 1,0\rangle \lvert)$	α_0^1	$-(1/21)^{1/2}$	$\alpha_0^1\begin{bmatrix} 0 & i/\sqrt{2} & 0 \\ -i/\sqrt{2} & 0 & 0 \\ 0 & 0 & 0 \end{bmatrix}$

[a] For $^7F_2$, $\alpha = -11/315$ and $\beta = 2/189$. For $^7F_1$, $\alpha_1 = -1/2$.

[b] All the A_n^m are expressed in cm^{-1}.

A complication is observed for lanthanide ions with an odd number of electrons. The assignment of the crystal field levels with respect to the symmetry of the scattering tensor elements and the wave functions is now based on irreducible representations for binary groups. All the crystal field levels are Kramers doublets and the double degeneracy may be removed when the ions are placed in a magnetic field. Table 4 gives the tensors and designations of the Raman lines shown for two Ce^{3+} transitions in $CeCl_3$—one from the $J_Z = \pm 5/2$ level to $J_Z' = \pm 3/2$ and another from the $J_Z = \pm 5/2$ level to $J_Z' = \pm 1/2$.

Thus, when a field is superimposed, it is possible to observe the individual components and the spectra for different polarisations may be constructed on the basis of the contributions of the scattering tensors to individual transitions. For one of the transitions in a zero field, the tensor is somewhat asymmetric. The frequency dependence of the degree of antisymmetry for the Ce^{3+} ion in $CeCl_3$ has been calculated[29]. It is illustrated in Fig. 9. The results depend greatly on the position of $\tilde{\nu}_{\chi k}$ which is ν_{4f5d} in our case. The presence of Kramers doublets in fact leads to a scattering tensor which differs from the normal tensors. Table 5 lists the characters of the binary group D_2 representations. All the crystal field states of the split LST manifold of a lanthanide ion with an odd number of f electrons belong to the representation Γ_5. Thus the transformation properties of the irreducible tensors $\Gamma_{\alpha_Q^K}$ are contained in the direct product of the representations $\Gamma_5 \times \Gamma_5 = \Gamma_1 + \Gamma_2 + \Gamma_3 + \Gamma_4$. The resultant overall tensor is therefore more complicated than the tensor for the vibrational transition of the system, which belongs to the usual point group D_2.

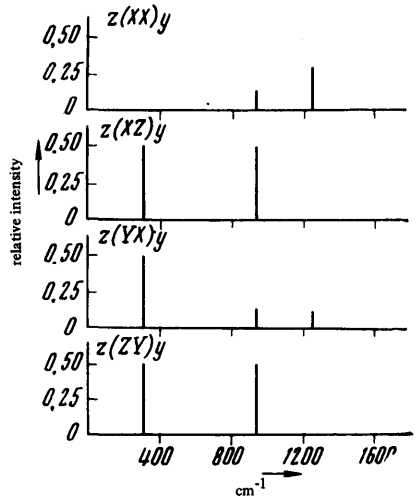


Figure 5. Calculated spectra of the tervalent europium ion in a crystal field of cubic symmetry for different polarisations. The intensities of the Raman lines with frequencies of about 800 cm^{-1} in Figs. 5 and 6 should be divided by 30 if the first excited electronic configuration has an energy of about 110 000 cm^{-1}. The crystal field parameters are $A_4^0 = -250$ cm^{-1} and $A_4^4 = 5A_4^0$, where $A_n^m = \langle r^n \rangle B_\Gamma^m$.

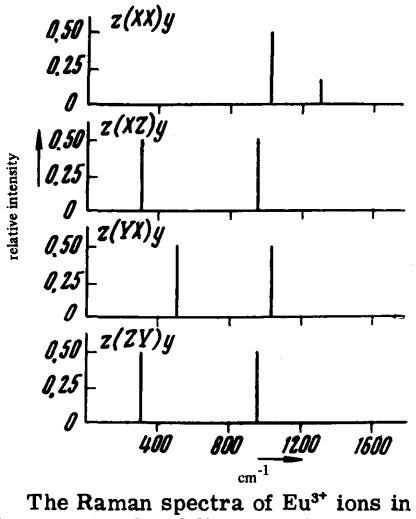


Figure 6. The Raman spectra of Eu^{3+} ions in a field with hexagonal symmetry for different polarisations. The crystal field parameters are $A_2^0 = 250$ cm^{-1} and $A_4^0 = -250$ cm^{-1}.

The calculation of the Raman spectrum for a specific polarisation presented here presupposes that the crystal unit cell contains one lanthanide ion and that the local axes of this ion are parallel to the macroscopic axes of the crystal. In most cases the situation is more complicated: the unit cell may contain more than one ion and the ions may occupy different sites with their own crystal field symmetry.

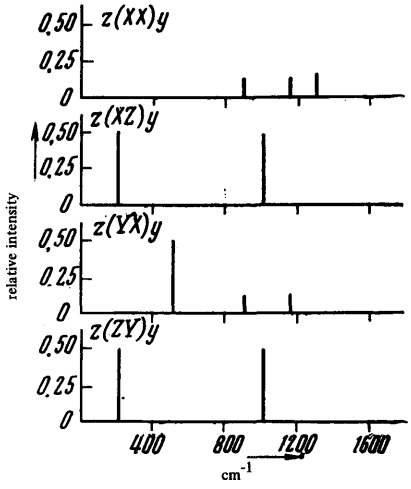


Figure 7. The Raman spectra of Eu^{3+} ions in a crystal field of tetragonal symmetry for different polarisations. The crystal field parameters are $A_2^0 = 250\ cm^{-1}$, $A_4^0 = -250\ cm^{-1}$, and $A_4^4 = -1000\ cm^{-1}$.

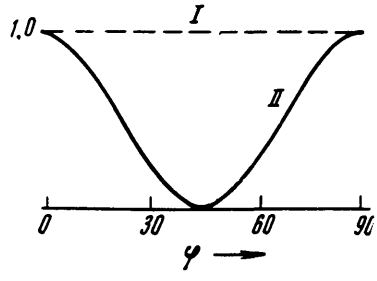


Figure 8. Variation of the Raman line intensity determined by the tensor element α_{yz} with the angle of rotation $\varphi°$ about the z axis of the crystal. Curves I and II refer to the asymmetric tensor $\begin{matrix} 0a0 \\ -a\,0\,0 \\ 0\,0\,0 \end{matrix}$ and the symmetric tensor $\begin{matrix} 0a0 \\ a\,0\,0 \\ 0\,0\,0 \end{matrix}$ respectively.

It is readily seen that the characteristics of the scattering by lanthanide ions are obtained for the entire crystal by the transformation of the scattering tensors $(\alpha_{\rho\sigma})^S_{kn}$ for each of the ions occupying different sites S in the laboratory coordinate system. This can be done with the aid of the rotation matrices R_S and R_S^{-1}, subsequent squaring of the individual tensor components, and their addition. The following scattering tensor is then obtained for the crystal:

$$[(\alpha_{\rho\sigma})_{kn}]^2_{\text{crystall}} = \sum_{\text{sites}} [R_s\,(\alpha_{\rho\sigma})^S_{kn} R_s^{-1}]^2.$$

Although this procedure is simple, it is clear that the interaction between various lanthanide ions is not taken into account. Indeed, it is possible to consider this case as one where there is incoherent scattering by the ions, in contrast to the case of coherent scattering. As has been shown by the present author and Schaack[12] it is then important to take into account the similarity between the factor-group interaction and the correlation between various phases of the scattering centres—lanthanide ions.

Table 4. The eigenvalues, eigenvectors, and Raman line intensities for the $^2F_{5/2}$ set of levels in a hexagonal crystal field.

$J_z - J'_z$ transition	Energy	Controlling element α_Q^K	$\alpha_Q^K/F(K,\nu)$	Intensity matrix
$-\frac{5}{2} \to -\frac{5}{2}$	$\frac{2}{3}\frac{4}{5}A_2^0 - \frac{3}{2}\frac{2}{1}A_4^0$	$\alpha_1^1 A_1^2$	$-\frac{2}{7}\sqrt{10/21}$	$\begin{bmatrix} 0 & \frac{1}{2}(a-b)^2 & \frac{1}{2}(a-b)^2 \\ \frac{1}{2}(a+b)^2 & 0 & 0 \\ \frac{1}{2}(a+b)^2 & 0 & 0 \end{bmatrix}$
			$\frac{6}{7}\sqrt{1/14}$	
$\frac{5}{2} \to \frac{3}{2}$	$\frac{2}{3}\frac{4}{5}A_2^0 - \frac{3}{2}\frac{2}{1}A_4^0$	$\alpha_{-1}^1 \alpha_{-1}^2$	$\frac{2}{7}\sqrt{10/21}$	
			$\frac{6}{7}\sqrt{1/14}$	
$-\frac{5}{2} \to -\frac{1}{2}$	$\frac{4}{3}\frac{6}{5}A_2^0 + \frac{3}{2}\frac{4}{1}A_4^0$	α_2^2	$\frac{3}{7}\sqrt{1/7}$	$\begin{bmatrix} \frac{1}{4}c^2 & \frac{1}{4}c^2 & 0 \\ \frac{1}{4}c^2 & \frac{1}{4}c^2 & 0 \\ 0 & 0 & 0 \end{bmatrix}$
$\frac{5}{2} \to +\frac{1}{2}$	$\frac{4}{3}\frac{6}{5}A_2^0 + \frac{2}{2}\frac{4}{1}A_4^0$	α_{-2}^2	$\frac{3}{7}\sqrt{1/7}$	

Table 5. The active representations for the D_2 binary group.

Representation	Components in cartesian coordinates	Irreducible components
Γ_1	$\alpha_{xx}, \alpha_{yy}, \alpha_{zz}$	α_2^2, α_0^0
Γ_2	$\alpha_{xy} \pm \alpha_{yx}$	$\alpha_2^2 - \alpha_{-2}^2, \alpha_0^1$
Γ_3	$\alpha_{xz} \pm \alpha_{zx}$	$\alpha_1^2 + \alpha_{-1}^2, \alpha_1^1$
Γ_4	$\alpha_{yz} \pm \alpha_{zy}$	$\alpha_{-1}^2 + \alpha_{-1}^2, \alpha_{-1}^1$
Γ_5	all the levels of the crystal field of the LSJ manifold	

Suppose that $\mathcal{H}_0$ is the Hamiltonian of an ion with a definite local symmetry, Φ_{ks} the wave function for the state k, and H_i the perturbation Hamiltonian describing the interionic energy. In the space group symmetry operations, H_i is transformed in the same way as H_0. The eigenfunctions Ψ_k for the $H_0 + H_i$ states with $k = 0$, which are important and of interest only in the case of first-order Raman scattering considered here, belong to an irreducible representation of the factor-group. In

terms of the zeroth approximation, these wave functions have the following form

$$\Psi_k = (1/N)\sum_s A_{ks}\Phi_{ks}.$$

With the exception of A_{ks}, these symbols have the usual significance. The A_{ks} are constants which have been chosen in such a way that the wave functions Ψ_k have been transformed in terms of the factor-group representations. Evidently the determination of A_{ks} is of primary importance.

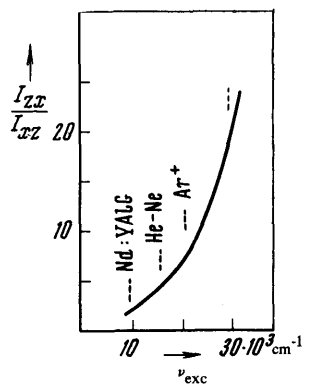


Figure 9. The ratio of the intensities I_{ZX} (related to the α_{ZX} element) and I_{XZ} (related to the α_{XZ} element) for Raman scattering in the electronic transitions of the Ce^{3+} ion in $CeCl_3$ for various frequencies of the exciting radiation.

For example, it follows from Table 6 that there is a unique relation between the representations of the local group D_2 and those of the factor-group O_h, since the representations of the group C_h appear once in each case. This makes it possible to set up the wave functions Ψ_k on the basis of symmetry considerations alone. If the irreducible representation γ is one-dimensional, then A_{ks} will be a character of γ referring to the symmetry elements which transform the site k into the site s. For two- or three-dimensional representations, it is necessary to employ the rules for finding the symmetry coordinates employed in molecular physics[17].

Table 6. Relation between the local irreducible representations and the representations of the factor-group for lanthanide ions in garnets.

D_2 representations	O_h^a representations	D_2 representations	O_h^a representations
A	$A_{1g}+E_g+T_{2g}$	B_2	$T_{2g}+T_{1g}$
B_1	E_g+T_{1g}	B_3	$T_{2g}+T_{1g}$

[a]Only the transformation properties of the Raman scattering tensor are quoted.

If the wave functions Ψ_k are used to calculate in the usual way (the integral $\langle\Psi_n|\alpha|\Psi_k\rangle \neq 0$) the scattering tensor components, the tensor for the crystal unit cell may be evaluated by the superposition of site tensors but now one must take into account the different phase factors. In this instance one must also consider the orientation of local axes, the following expression being obtained for the Raman intensity:

$$[(\alpha_{\rho\sigma})_{kn}]^2_{\text{crystal.}} = \Big[\sum_{\text{sites}} A^*_{ns}A_{ks}R_s \times (\alpha_{\rho\sigma})^s_{kn}R_s^{-1}\Big]^2.$$

The angles of rotation, which are important for the R_S and R_S^{-1} matrices for different sites of the unit cell, are obtained most simply when the directions of the local axes are known.

Calculation of the incoherent and coherent scattering tensors leads in general to the same results, but there is also a difference. In the first case one finds that the tensor for the Raman lines is determined by tensors associated with definite representations of the factor-group. It is then impossible to obtain information about the site tensors. On the other hand, in the case of coherent scattering, such information may be obtained and there is a relation between the crystal scattering matrix elements and the analogous values for the sites.

V. THE BREAKDOWN OF SELECTION RULES

In previous sections it was stated that the low electronic levels of the tervalent europium ion belong to the states ^7F_J, where $J = 0, 1, 2, \ldots, 6$. The $^7F_0$ state is the lowest and the $^7F_1$, $^7F_2$, and $^7F_3$ states are at about 300, 900, and 1800 cm^{-1} respectively.

The selection rules for electronic Raman scattering of lanthanide ions are as follows[4,5]: $\Delta S = 0$, $\Delta L \leqslant 2$, and $\Delta J \leqslant 2$; according to the $\Delta J \leqslant 2$ rule[4], the $^7F_0 - {}^7F_3$ transition is forbidden. However, this selection rule is valid only when J can still be regarded as a "good" quantum number, i.e. in those cases where the distances between the crystal field components are small compared with the distances between the energy levels for the state of the free ion. For strong crystal fields, "good" quantum numbers yield only the representations of the local symmetry group, so that different values of J may become mixed in a single eigenstate. However, the mixing of the J depends not only on the strength of the crystal field but also on its symmetry, since certain values of J cannot become mixed in the crystal if the crystal field symmetry is sufficiently high (for example states with $J = 0$ and $J = 3$ are not mixed for D_4 symmetry). Thus a good example of the breakdown of the $\Delta J \leqslant 2$ rule is provided by a crystal with a strong crystal field and a low local symmetry of the lanthanide ion. Among all the lanthanide ions, the free Eu^{3+} ion has the lowest levels; in this case mixing of the J can be achieved most readily. On the other hand, the aluminate crystal matrix gives rise to a strong crystal field with the point group having the C_S symmetry for the position of the lanthanide ion[6]. Table 7 shows that the states of the crystal fields with $J = 3$ belongs to the representations A' (Hougen and Singh[3]) and A'' (Elliott and Loudon[4]), but the wave functions of these states presumably contain an admixture of states with other values of J (particularly with $J = 2$). As a result, the Raman scattering in the $^7F_0$—$^7F_3$ electronic transition becomes allowed and the non-zero components of the scattering tensor again belong to the representations A' and A'' of the group C_S. It is possible to show in the same way that the Raman scattering in the $^7F_0$—$^7F_4$ transition is also allowed, but the intensity of these transitions

will presumably be much lower, because (1) the difference between the energies of the $^7F_2$ and $^7F_4$ levels is now about 2000 cm^{-1} and the states are mixed to a smaller extent than are the $^7F_3$ and $^7F_2$ levels where $\Delta E \simeq 800$ cm^{-1} and (2) the Raman intensity is proportional to the fourth power of the frequency of the emitted radiation.

Table 7. Symmetry properties of the crystal field levels for the ^7F_J set of $EuAlO_3$.

^7F Set	Representations of C_S groups	^7F Set	Representations of C_S groups
0	A'	2	$2A' + 3A''$
1	$A' + 2A''$	3	$3A' + 4A''$

α_{xx}, α_{yy}, α_{zz}, and α_{xy} enter into A'. α_{yz} and α_{xz} enter into A''.

The effect of the mixing of the J states has also certain interesting consequences for antisymmetric and isotropic tensors. Eu^{3+} ions provide a good example of the former. According to theory, the $^7F_0 - ^7F_2$ transitions are related to the more usual symmetric tensors. If the wave functions of the $^7F_1$ and $^7F_2$ states are mixed, then evidently the scattering tensors for the $^7F_0 - ^7F_1$ transitions now become partly antisymmetric and correspondingly some of the tensors for the $^7F_0 - ^7F_2$ transitions may change from symmetric to partly antisymmetric. The degree of antisymmetry depends on the percentage admixture of the corresponding states. The isotropic scattering tensor α_0^0 cannot contribute to transitions for the free ion either within the limits of a single configuration or to interconfigurational transitions. This follows from an examination of the conditions for a non-zero value of the 3j-symbol introduced previously. However, as in the breakdown of the selection rule for the transitions with $\Delta J = 3$ and 4 in Raman scattering, the isotropic tensor can also contribute to the intensity under the influence of the mixing of the J states. From the theoretical standpoint, it is useful to recall that the absolute magnitude of $|\alpha_0^0|$ is about 100 times greater than $|\alpha_Q^{1,2}|$ and in the case of $^7F_0 - ^7F_2$ transitions it is easier to observe the presence of the isotropic tensor than that of the antisymmetric tensor.

In formulating the expressions for the scattering tensor, it was postulated that the frequency of the incident radiation (ν_0) is strongly displaced in relation to the frequency of the absorption band of the system. In this instance, when ν_0 is close to the value for the absorption band of the lanthanide ion, the Raman intensity for the transition between the ground stage g and the final state e is determined by the following scattering tensor:

$$(\alpha_{\rho\sigma})_{gl} = \sum_r \frac{\langle e|\rho|r\rangle\langle r|\sigma|g\rangle}{h\nu_0 - h\nu_{gr} + i\gamma_r} + \frac{[\rho \leftrightarrow \sigma]}{h\nu_0 + h\nu_{rl} + i\gamma_r} \quad . \qquad (19)$$

Here $\langle e|\rho|r\rangle$ and $\langle r|\sigma|g\rangle$ are the matrix elements of the operators ρ and σ of the electric dipole moment (ρ, $\sigma = x$, y, z; γ is the decay operator related to the line width of the electric dipole transition from the state g to the state r). In the derivation of Eqn. (19), we must assume that the matrix elements of the dipole operator become zero for transitions between states of the same parity. Thus only transitions between states with the $4f^n5s^25p^6$ configuration contribute, since owing to the crystal field states with configurations of other parities, similar to $4f^{n-1}5s^25p^65d$, become mixed in. If we designate by $|\alpha\rangle$ the lowest (as regards energy) configuration $|4f^n5s^25p^6\rangle$ and by $|\beta\rangle$ the first of the higher configurations $|4f^{n-1}5s^25p^65d\rangle$ of opposite parity, then one can write for the low states of the crystal field

$$|\Psi_1\rangle = a_1|\alpha\rangle + b_1|\beta\rangle + \ldots,$$
$$|\Psi_2\rangle = a_2|\alpha\rangle + b_2|\beta\rangle + \ldots,$$

where $a_1 \simeq a_2 \simeq 1$, $b_1 \simeq b_2 \simeq V_C/(E_\beta - E_\alpha)$, V_C determines the crystal field strength, and $E_\alpha - E_\beta$ determines the energy difference between the two configurations, equal to approximately 10^5 cm^{-1}. Here we are dealing with cases where V_C is between 10^2 and 10^3 cm^{-1} Then the values of b_1 and b_2 are also somewhere between 10^{-3} and 10^{-2}.[3]

An estimate of the matrix elements of the dipole moment operator is

$$\langle\Psi_1|\rho|\Psi_2\rangle \approx (a_1b_2 + b_1a_2)\langle\alpha|\rho|\beta\rangle \approx 10^{-2} \div 10^{-3}\langle\alpha|\rho|\beta\rangle.$$

Resonance implies that $\nu_0 \simeq \nu_{gr}$ and, if one assumes that the denominator of the first term in Eqn. (19) becomes equal to approximately ten, then this term has an order of magnitude somewhere between 10^{-5} and 10^{-7} in units of $|\langle\alpha|\rho|\beta\rangle|^2$. The second term in Eqn. (19) may be neglected.

If we consider the part of the sum for which the intermediate state $|r\rangle$ belongs to the configuration $4f^{n-1}5s^25p^65d$, then the denominator, which depends on the energy, will be 10^5 and we obtain 10^{-5} in units of $|\langle\alpha|\rho|\beta\rangle|^2$ for the contribution of this part of the sum. Hence we see that, although the matrix elements $\langle\Psi_1|\rho|\Psi_2\rangle$ are in fact very small, they can have an appreciable influence in the case of resonance. One can reach the following two conclusions.

1. The resonance effect depends on the admixture of states with a different parity from the states of the lowest conformation of the crystal field and consequently should be more intense for stronger crystal fields.

2. When the symmetry point group contains an inversion centre, there should be no resonance effect, since a crystal field of this type does not involve the mixing of configurations of different parities.

The matrix element $\langle\Psi_1|\rho|\Psi_2\rangle$ depends also on whether ρ is equal to x, y, or z. Thus the properties of the polarisation of the transition from the ground state to the resonance state have a direct influence on the Raman scattering tensor. In the special case where a direct transition between the two states is forbidden, we would not observe any resonance effect. However, the corresponding absorption line will of course also be missing under these conditions.

VI. EXPERIMENTAL METHODS

The apparatus for the investigation of Raman scattering is illustrated schematically in Fig. 10. It can be seen that the direction of propagation of the laser radiation is at right angles to the direction of the scattered light. In the general case the laser is focused in a very narrow beam within the crystal. Estimates of the beam diameter in our experiments yielded about 150—200 μm. The crystal was placed at the top of the cold finger of the experimental helium Dewar vessel fitted with windows for the illumination of the specimens and the observation of the scattered light. The light from the laser beam within the crystal was reflected onto the slit of a double monochromator.

Double monochromators are now used in Raman spectroscopy, since they are particularly effective in eliminating the scattered light and make it possible to observe Raman lines displaced by less than 10 cm^{-1} from the unperturbed Rayleigh line. In most cases a photomultiplier is used as a detector; in our experiments we employed a photomultiplier with an S20 cathode. The signal from the photomultiplier was transferred to an integrating digital voltmeter, the time constant of which was set in the range from 1 to 60 s. By reducing the scanning rate of the monochromator to 1.25 Å min^{-1}, it is possible to employ time constants of about 20 s. In order to prevent the distortion of the line form of the radiation, the slit width S, the time constant t, and the scanning rate v must be related as follows: $tv/S = 1/2$. The details of the detector are shown schematically in Fig. 10. A photomultiplier of type EMI 9558B was used in the experiments. The solenoid was placed directly around the photocathode; the light emerging from the output slit of the monochromator was focused by lenses onto a small section of the photocathode. The magnetic lines of force generated by the solenoid prevented the incidence on the first dynode of the photoelectrons emitted from different parts of the cathode, except its centre on which the scattered light impinged. This gave rise to an effective amplification of the signal to noise ratio by a factor of approximately six compared with the case where the magnetic field was switched off and the entire area of the photocathode was illuminated. The crystals employed in the experiments were very small and the length of the path traversed by the laser beam within the crystal hardly exceeded 4 mm in all cases. It is well known that the width of the electronic levels depends greatly on the temperature of the specimen. The lower the temperature, the smaller the width of the electronic level. For this reason, transitions between electronic levels were investigated at low temperatures.

However, such investigations suffer from the disadvantage that the principal characteristic of the Raman spectrum, the presence of anti-Stokes and Stokes lines, is lost if the specimen is cooled to very low temperatures. Nevertheless, for electronic levels in the region up to 150 cm^{-1} even at specimen temperatures below 77°K, there are excited lines with sufficient populations to ensure an adequate intensity of the anti-Stokes spectrum. In order to determine which line in the Raman spectrum of the crystal is due to Raman scattering in an electronic transition, the phonon spectrum of the lattice-matrix was compared, for example, with the spectrum of a lanthanide compound. The appearance in the latter of new lines might have been an indication that Raman scattering in electronic transitions takes place. However, the study of the phonon spectra of lanthanide compounds of the garnet type showed that marked differences are observed in the positions of the phonon bands for different lanthanide garnets. This implies that additional lines observed in the spectra of lanthanide compounds are not necessarily electronic Raman lines. A reliable method for determining which lines in the Raman spectrum belong to electronic transitions involves placing the specimen in strong magnetic fields. The low electronic levels of lanthanide ions in the crystal are sensitive to the influence of external magnetic fields; this is of course not the case for phonon lines. Fig. 10*c* presents details of the experimental apparatus in which the crystal is placed within a superconducting magnet fitted with the necessary apertures whereby it is possible to illuminate the crystal with laser light and to observe the scattered radiation at right angles to the direction of propagation of the laser beam. The specimen

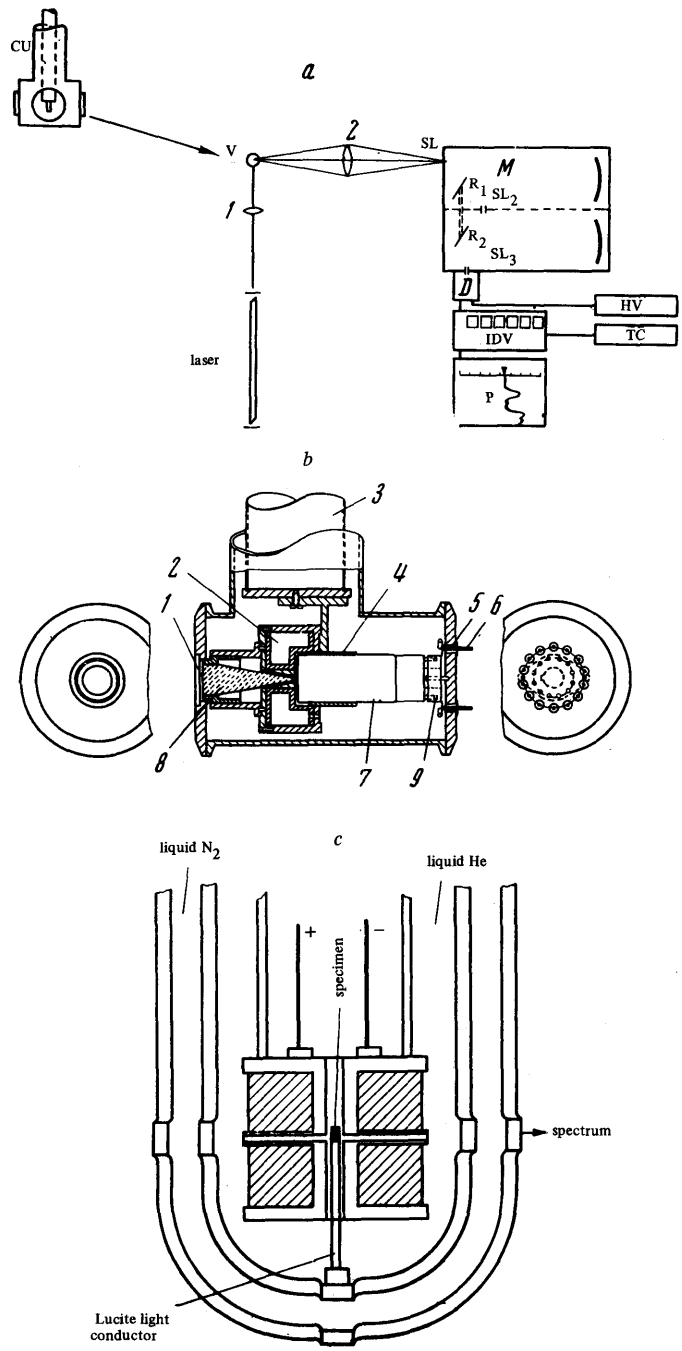


Figure 10. *a*) Diagram of apparatus for the measurement of Raman spectra with laser excitation: V—Dewar vessel containing the single crystal [the laser radiation is focused by the lens (*1*) into the interior of the crystal]; D—detector; HV—high voltage source; IDV—integrating digital voltmeter; P—pen recorder; TC—device for the measurement of the voltmeter time constant; M—double monochromator; CU—cuvette; SL—slit; R—replica gratings. *b*) Detector with cooling system and magnetic defocusing: *1*) Pyrex window; *2*) coil; *3*) to Dewar vessel; *4*) copper tube; *5*) glass—metal seal; *6*) photomultiplier terminals; *7*) photomultiplier; *8*) Pyrex light conductor. *c*) Schematic illustration of the position of the specimen in the superconducting magnet.

is now immersed in liquid helium and, needless to say, at this low temperature the anti-Stokes Raman lines should not be observed. An advantage of experiments at such temperatures is of course that the electronic levels under these conditions are very narrow. Care must be taken to screen the photomultiplier from the magnetic field generated by the superconducting magnet.

Having discussed the theory and the experimental conditions in the study of electronic Raman scattering, we now proceed to Section VII, which discusses the experimental aspects of electronic Raman spectroscopy.

VII. EXPERIMENTAL RESULTS‡

The Raman spectra of lanthanide ions in single crystals are discussed in this section. Consequently, apart from the excitation of the electronic levels, the phonons of the crystal–matrix will play a certain role. In the theoretical Section IV it was shown that the scattering cross-section for electronic transitions is lower than for vibrational Raman scattering and therefore it is more convenient to investigate lanthanide compounds which contain a high percentage of lanthanide ions. Such systems may be found in the series of rare-earth chlorides ($RECl_3$) [3,30] or their aluminates ($REAlO_3$). The phonons for the latter lattice-matrix are observed at frequencies <600 cm^{-1} and Fig. 11 illustrates part of the $SmAlO_3$ spectrum containing Raman lines in the range 1000–1550 cm^{-1}. According to the energy level diagram presented in Fig. 1, transitions of the type $^6H_{5/2} - {}^6H_{7/2}$ are to be expected in this region. The width of these transitions depends on the crystal temperature, which distinguishes between them and phonons and the data presented in Fig. 11 make it possible to establish immediately the position of the four crystal field components for $J = 7/2$. Raman scattering in electronic transitions within the limits of the $^6H_{5/2}$ configuration cannot be observed as they coincide in position with the intense phonons of the aluminate crystal. Another example of such systems has been found in the series of RE_2O_3 crystals[31]. The compounds Yb_2O_3 and Er_2O_3 were investigated and electronic transitions at a frequency of about 41 cm^{-1} were found for the erbium compound. The phonon level of the Yb_2O_3 and Er_2O_3 crystals differ also in their width which may indicate the occurrence of an electron–phonon interaction. The crystals of lanthanide oxides are cubic, another series of crystals of the same symmetry being provided by lanthanide garnets. Here we are interested in the lanthanide aluminium and gallium garnets with the general formulae $RE_3Al_5O_{12}$ or $RE_3Ga_5O_{12}$. The unit cell contains 80 atoms and the 237 degrees of freedom of the species may lead to a complex spectrum. By virtue of the cubic symmetry of the crystals, the appearance of only 21 vibrations active in Raman scattering is expected in the spectrum; the corresponding lines were observed in the spectra of many crystals containing aluminium and gallium in the range 40–900 cm^{-1}. Thus, as for the aluminates, here too it is convenient to investigate the electronic effects outside the phonon region.

Fig. 12 presents the spectra for different polarisations of the compound $Tb_3Al_5O_{12}$ with cubic symmetry. The spectrum arises as a result of transitions from the ground state (which is one of the levels of species $^7F_6$) to levels of species $^7F_5$. The local symmetry of the lanthanide ions in the garnet crystals is determined by the point group with D_2 symmetry since all the levels belong to one of the representations A, B_1, B_2, or B_3 of this group. For a transition of the type $A(^7F_6)$–$A(^7F_5)$, the tensor is determined by components transformed in accordance with the representations $A_{1g} + E_g + T_{2g}$; the tensor is the same also for transitions between levels with the symmetry $B_1(^7F_6)$ and $B_1(^7F_5)$, etc.§ However, since the symmetry of the crystal field is known, it is possible to predict how many times tensors of the type $A_{1g} + E_g + T_{2g}$, $E_g + T_{1g}$, and $T_{2g} + T_{1g}$ will appear. By altering the illumination conditions, it is possible to show that the symmetry of the ground state is A or B_1.

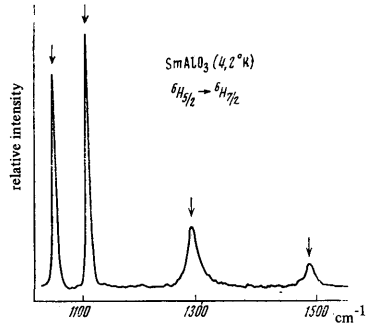


Figure 11. Low-temperature Raman spectrum of a non-oriented $SmAlO_3$ single crystal; the arrows indicate the $^6H_{5/2}$–$^6H_{7/2}$ electronic transitions.

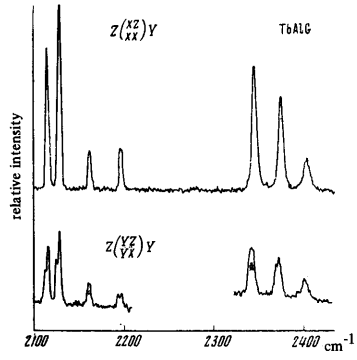


Figure 12. Raman spectrum of terbium aluminium garnet at 4.2°K. The lower spectrum is that of a crystal placed in a magnetic field of about 2.5 kG. •

Having thus at one's disposal two possible sets for the assignment of states of the type $^7F_5$ in a crystal field with D_2 symmetry, it is now possible to employ the mathematical procedure used in crystal field calculations. In such calculations it was assumed that the ground state has the A symmetry and that the excited state with B_1 symmetry lies more than 10 cm^{-1} above the ground state.

‡ The results presented in this section have been selected from data which have already been published[3,10,18,19,21,23].

§ See also Table 6.

It is most convenient to assign particular symmetries to the electronic levels using a spectroscopic technique based on electronic Raman scattering. The transitions in luminescence or absorption are usually largely related to the electric dipole moments and the moments in the directions x, y, and z for a cubic crystal cannot be distinguished. The dipole moment operator is transformed in accordance with one of the representations of the factor-group and therefore one cannot achieve a symmetry assignment for the crystal field levels. The electronic transitions for the $^7F_5$ levels in Raman scattering have frequencies below 600 cm^{-1} and this region also contains the phonons of the garnet crystal. Electronic Raman scattering can be separated from the phonon spectrum by comparing the spectrum in Fig. 13 with that of the yttrium–aluminium garnet. The positions of the corresponding phonons for the two crystals are established with the aid of identical polarisation measurements in Raman spectra. The high intensities of the electronic transitions in the range from 60 to 90 cm^{-1} are somewhat surprising. The general conclusion from data for TbAlG is that not all possible electronic transitions are observed. Evidently the width of the transitions continues to increase if the difference between the energies of the electronic levels reckoned from the lowest set of levels increases. Thus the width of the excited levels remote from the lowest level may be so great that it is difficult to observe the transitions, particularly if the phonons of the crystal-matrix are present.

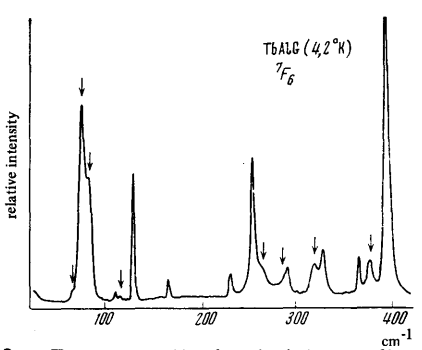


Figure 13. Raman scattering in interconfigurational electronic transitions of the type $^7F_6$ in TbAlG.

The foregoing considerations are confirmed by the data in Fig. 14. Like the main set of Tb^{3+} levels, Tm^{3+} ions also have the quantum number $J = 6$ in the ground state. Thus the crystal field with D_2 symmetry has 13 components but only two transitions have been observed for TmAlG. Under the same experimental conditions (power of the laser, quality of the crystal, recording system, etc.), it was found that the scattering at the electronic levels of the Tm^{3+} ion is definitely smaller than for the Tb^{3+} ion in the aluminium garnet crystal. This is at least consistent with the *ab initio* calculations of the absolute cross-sections presented in Table 2.

The changes in the spectra arising because the levels and the tensor components belong to representations of binary groups can be most satisfactorily demonstrated for $DyAl_5O_{12}$. The tensors for the phonons of this compound belong to the factor-group O_h. The space group of the garnet is O_h.[10] Fig. 15 illustrates part of the low-temperature Raman spectrum of DyAlG. Experiments showed that the upper spectrum is due to phonon (and electronic) levels with the E_g symmetry only. The lower Raman spectrum reflects only the transitions with T_{2g} symmetry. Evidently the phonons have the E_g or T_{2g} symmetry.

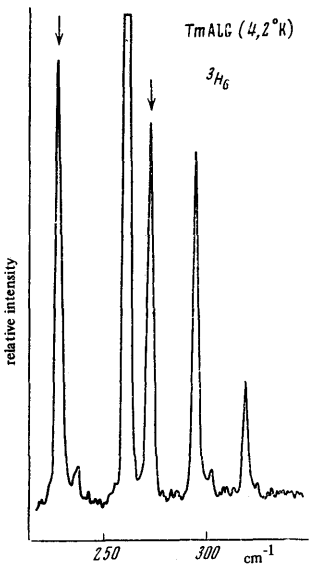


Figure 14. Raman scattering in two electronic transitions in thullium aluminium garnet.

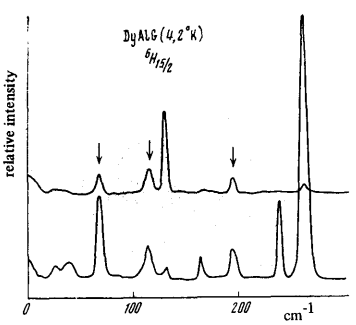


Figure 15. Polarisation Raman spectrum of an oriented crystal of dysprosium aluminium garnet. The difference between the polarisation characteristics of the electronic (↓) and phonon transitions becomes clear when the upper and lower spectrograms are compared.

The tensor for electronic transitions is contained in the representation $\Gamma_5 \times \Gamma_5 = \Gamma_1 + \Gamma_2 + \Gamma_3 + \Gamma_4$ of the binary group D_2 (see also Table 5). Thus we find that, as a result, the tensor for the transitions between electronic levels with Γ_5 symmetry no longer belongs either to the E_g representation or to the T_{2g} representation. This tensor is more complex and the spectra shown in Fig. 15

confirm the theoretical predictions. The Raman spectroscopic data for the electronic transitions in DyAlG have also been used to determine the crystal field strength expressed in terms of the coefficients A_n^m. The results of the calculation of the crystal field using data for electronic Raman scattering are important not only for the prediction on the basis of the crystal field parameters of the positions of the crystal field levels but also for the determination of the symmetry of the states. Thus there are more experimental data than the parameters to be determined and such data are now being used to find the parameters for all possible lanthanide garnets. Fig. 16 presents part of the Raman spectrum of $EuGa_5O_{12}$ (europium gallium garnet). According to theory, the observed electronic transitions of the type $^7F_0 - ^7F_1$ are due to a fully antisymmetric tensor. For cubic crystals, there are several methods for the determination of the tensor symmetry. It is impossible to distinguish symmetrical and antisymmetric tensors when the crystal is oriented in such a way that the excited radiation is propagated along the *a* axis of the garnet crystal and the scattered radiation is observed along the *b* and *c* axes. This situation differs radically from the case where the crystal is rotated by 45° about the *c* axis so that the direction of propagation of the incident radiation makes an angle of 45° with the *a* and *b* axes and the direction of observation of the scattered light is at right angles to them, as in all normal cases.

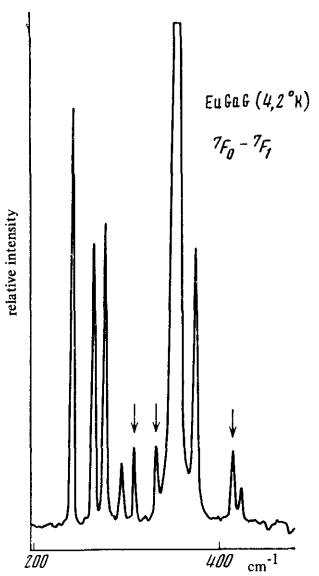


Figure 16. Electronic Raman scattering of Eu^{3+} in europium gallium garnet. The scattering corresponds to fully antisymmetric tensors.

Lanthanide ions occupy sites with D_2 symmetry and in the unit cell there are six such sites. Using the theory of the incoherent and coherent Raman scattering tensors, it is possible to set up the corresponding matrices taking into account the rotations; they are presented in Table 8.

Evidently, if the entire intensity is internally related to a phonon with E_g symmetry, then the intensity ratio $R = I_{yx+yz}/I_{zx+zz}$ becomes zero for the Raman line with A_g symmetry, 8/3 for the line with T_{1g} symmetry (antisymmetric tensors), and 4/3 for the line with T_{2g} symmetry (symmetrical tensors). The tensors which transform as the T_{1g} representation of the factor-group are of the form $(\alpha_{xy} - \alpha_{yx}, \alpha_{yz} - \alpha_{zy}, \alpha_{xz} - \alpha_{zx})$ and those which transform as the T_{2g} representation are $(\alpha_{xy} + \alpha_{yx}, \alpha_{yz} + \alpha_{zy}, \alpha_{xz} + \alpha_{zx})$.

Table 8. Scattering matrices for an oriented EuGaG crystal.

Tensor symmetry	Scattering matrix	Tensor symmetry	Scattering matrix
A_{1g}	$\begin{bmatrix} a^2 & & \\ & a^2 & \\ & & a^2 \end{bmatrix}$	T_{2g}	$\begin{bmatrix} c^2 & 0 & c^2 \\ 0 & c^2 & c^2 \\ c^2 & c^2 & 0 \end{bmatrix}$
E_g	$\begin{bmatrix} b^2 & 3b^2 & 0 \\ 3b^2 & b^2 & 0 \\ 0 & 0 & 4b^2 \end{bmatrix}$	T_{1g}	$\begin{bmatrix} 0 & d^2 & d^2 \\ d^2 & 0 & d^2 \\ d^2 & d^2 & 0 \end{bmatrix}$

It has been found experimentally that $R = 2.6 \pm 7\%$ for the 308 cm^{-1} line and $R = 2.6 \pm 10\%$ for the 329 cm^{-1} line. Owing to the presence of the phonon with T_{2g} symmetry close to the electronic transition at 411 cm^{-1}, it is impossible to determine the ratio R in this case. The experimental results show that two of the $^7F_0 - ^7F_1$ transitions indeed involve antisymmetric tensors. The first electronic Raman spectrum obtained on laser excitation was that of yttrium gallium garnet doped with europium[6] so that it is now evident that transitions due to the antisymmetric tensor were recorded as early as 1966.

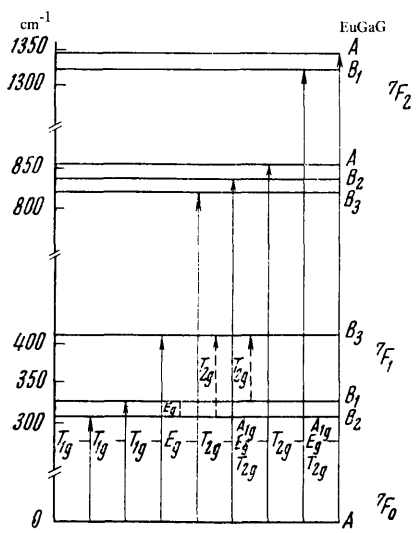


Figure 17. Low energy levels of Eu^{3+} in EuGaG.

Raman scattering has also been observed in electronic transitions of the type $^7F_0 - ^7F_2$; according to theory,

these transitions are linked to symmetrical tensors. The low energy levels of EuGaG obtained from Raman spectroscopic data are presented in Fig. 17. The presence of a level with B_1 symmetry in the gap between the levels with B_3 and B_2 symmetries for $^7F_1$ suggests that the crystal field is orthorhombic and the deviation from tetragonal symmetry is large. Thus, although the crystal is in fact cubic, the europium ion is in a crystal field determined by the local orthorhombic symmetry. Using in the analysis the mathematical procedures of the crystal field theory, it is possible to calculate the eigenvectors of the crystal field levels; the results of the calculation are presented in Table 9.

Table 9. Energies and assignments with respect to symmetry and the wave functions of the low-lying ^7F set of energy levels for EuGaG.

^7F_J State	Absorption of fluorescence	Frequency of Raman lines, cm^{-1}	Calc.[a]	Symmetry	Symmetry in terms of the basis function in $\|gJ_z\rangle$
$^7F_1$	305	308	308	B_2	$(1/\sqrt{2})(\|1_g1\rangle+\|1_g{-}1\rangle)$
	328	329	330	B_1	$\|1_g0\rangle$
	407	411	412	B_3	$(1/\sqrt{2})(\|1_g1\rangle-\|1_g{-}1\rangle)$
$^7F_2$		819	854	B_2	$(1/\sqrt{2})(\|2_g1\rangle-\|2_g{-}1\rangle)$
	833	834	869	B_3	$(1/\sqrt{2})(\|2_g1\rangle+\|2_g{-}1\rangle)$
	870	855	899	A	$\|20\rangle, (1/\sqrt{2})(\|2_g2\rangle+\|2_g{-}2\rangle)$
	1294[b]				
	1324	1324	1265	B_1	$(1/\sqrt{2})(\|2_g2\rangle-\|2_g{-}2\rangle)$
	1343	1341	1286	A	$\|20\rangle, (1/\sqrt{2})(\|2_g2\rangle+\|2_g{-}2\rangle)$
$^7F_3$	1830[b]	1832			
	1851[b]	1853			
	1894[b]	1896			
	1925[b]	1929			
	1977[b]	1982			
	2068[b]	1982			

[a] Calculation without taking into account the mixing of the J states for the following values of the parameters: $A_2^0 = -50$, $A_2^2 = 260$, $A_4^0 = -330$, $A_4^2 = 275$, $A_4^4 = 1400$.

[b] According to the data of Sonnich-Mortensen, and Koningstein[14].

Table 10. Fluorescence line frequencies at 77°K, Raman spectra, and frequency assignments for $EuAlO_3$.

Observed frequencies	Assignment	Energy of state, cm^{-1}	Raman line frequencies ($^7F_0 - {}^7F_J$)
17 208	$^5D_0$—$^7F_0$	$^7F_0$: 0	
16 944		264	274
16 859	$^5D_0$—$^7F_1$	$^7F_1$: 350	356
16 735		474	476
16 266		942	945
16 240		968	968
16 195	$^5D_0$—$^7F_2$	$^7F_2$: 1013	1009
16 169		1039	1034
15 939		1269	—
15 388		1820	1814
15 382		1826	1824
15 354	$^5D_0$—$^7F_3$	$^7F_3$: 1854	1856
15 306		1902	1900
15 267		1941	1942
15 256		1952	1952

Calculation of all the Raman lines presupposes, as stated in the theoretical section, a complete analysis of the diagrams of energy levels belonging to set ^7F_j.

The selection rule $\Delta J \leq 2$ for electronic transitions does not hold either for EuGaG or $EuAlO_3$. The results of the study of the Raman and fluorescence spectra of $EuAlO_3$ are presented in Table 10 and Fig. 18 also shows the spectra and the energy level diagram.

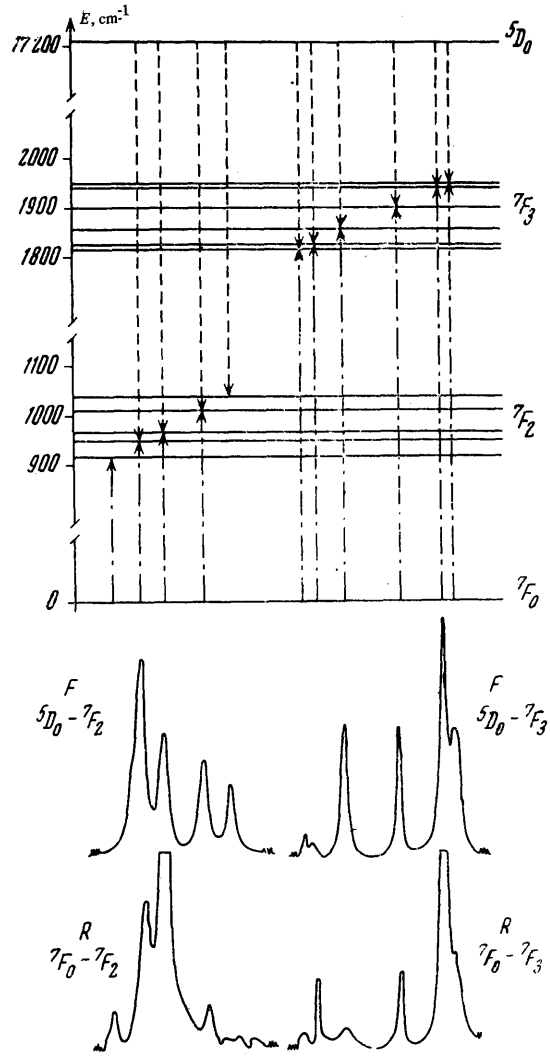


Figure 18. Transitions associated with the fluorescence and Raman scattering in europium aluminate.

The breakdown of the selection rule $\Delta J \leq 2$ occurs owing to the mixing of the J states, since the europium ion in the garnet and aluminate crystals is subjected to powerful crystal fields. The theory of the calculation of Raman intensities was applied to $CeCl_3$ and $PrCl_3$ crystals. A good agreement with experiment was found for $CeCl_3$. It was discovered that one of the Raman lines is linked with a partly asymmetric tensor. The calculated degree of asymmetry agrees satisfactorily with experimental data, possibly owing to the simplicity of the energy level scheme for Ce^{3+}. There is a good agreement between theory and experiment also for $PrCl_3$. The calculations are simple,

since the crystal field is determined by a small number of parameters.

We shall now turn our attention to the results of studies on resonance Raman scattering and the Zeeman effect in Raman scattering. The observation of electronic Raman scattering involved serious experimental difficulties. Firstly, it was necessary to find a system where at least one of the electronic absorption bands coincides with the available laser lines. The majority of absorption spectra of crystals with lanthanide ions contain a large number of lines in the green and blue regions of the visible spectrum and therefore there is some probability of a coincidence with the emission lines of the argon laser. Indeed a fairly large number of such cases have been found but only some of them are suitable for the investigation of resonance Raman scattering.

It was discovered that under these conditions not only the frequencies but also the oscillator strength of the chosen transition must satisfy special requirements. If the oscillator strength is too low, there is no interaction and consequently there is only a slight increase of the Raman intensity, while in the opposite case the entire exciting laser light is absorbed in a thin layer on the surface of the crystal. Although the resonance effect can in fact occur under these circumstances, the Raman scattering is too weak to be detected. Thus the optimal conditions should be sought when (a) the laser line coincides with an absorption band of moderate intensity and (b) when the specimen does not absorb in the part of the spectrum containing the Raman lines.

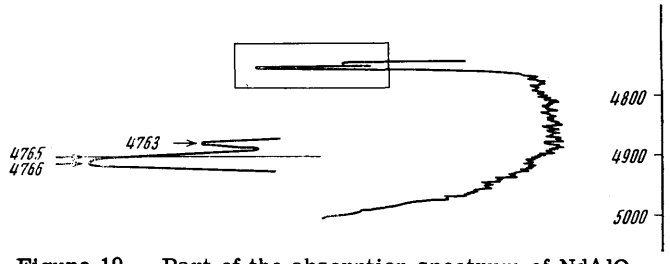


Figure 19. Part of the absorption spectrum of $NdAlO_3$ in the region of the 4765 Å line of the argon laser.

In our particular case the most serious difficulty involved making sure that the observed lines are indeed due to electronic Raman scattering and not to fluorescence. Fig. 19 presents the absorption spectrum of Nd^{3+} in $NdAlO_3$, which is involved in resonance with the 4765 Å line of the argon laser. Fortunately there is no complete coincidence in this case. The laser line is located at the wing of the absorption line on the high-energy side and it is displaced by approximately 4 cm^{-1} relative to its centre. If the observed emission lines (Fig. 20) were due to transitions caused by fluorescence from this level to lower levels, there would have been a 4 cm^{-1} shift relative to the Raman spectrum. Such a shift is not observed. The positions of the two low levels were known from the Raman spectrum obtained on excitation by the 4880 Å laser line; they were established for the first time by Scott[5]. Fig. 19 shows that there is a window in the absorption spectrum of the crystal between 4770 and 4950 Å. The intensity of the Raman lines in this region does not change owing to partial absorption. The Raman lines excited by those of the argon laser at wavelengths of 4765 and 4880 Å, which occur in this region, can therefore be compared directly with one another.

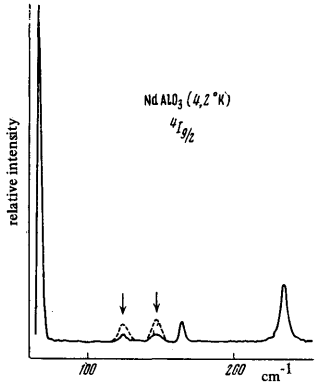


Figure 20. Raman spectrum of $NdAlO_3$ excited by light corresponding to the line at wavelengths of 4765 Å (shown dashed) and 4880 Å.

The spectra obtained with and without resonance, i.e. excited by laser lines at wavelengths of 4765 and 4880 Å, are compared in Fig. 20. The 53 and 147 cm^{-1} lines are due to phonons, while the 125 and 146 cm^{-1} lines are associated with electronic Raman scattering at the electronic levels. The phonon lines can be used as a standard in adjusting the spectra illustrated in Fig. 20 to the same intensity scale. Indeed the Raman spectrum excited by the 4765 Å line has a lower intensity owing to the partial absorption of the laser emission. Fig. 20 shows that the intensity of the electronic line increases approximately by a factor of five in the case of resonance. This small increase of intensity is inconsistant with the considerations put forward in Section V. It is found that not all the components of the scattering tensor increase in resonance Raman scattering. The symmetry of the resonating excited levels plays a role here, but, owing to the low symmetry of the $NdAlO_3$ crystal and because of the complexity of the tensor for scattering in electronic transitions (binary groups!), no attempts were made to determine the components of this tensor. Resonance scattering has also been observed for the Nd^{3+} ion in yttrium gallium garnet and for the Dy^{3+} ion in garnet crystals. All the data indicate that the dipole transitions within the limits of the $(4f)^n$ configuration have a weak influence on the elements of the scattering tensor for electronic transitions compared with the contributions having a direct bearing on the matrix elements. The case where the exciting line is in resonance with an interconfigurational transition has been observed for the Ce^{3+} ion in CaF_2; the enhancement of the electronic transitions was more marked, since the oscillator strength for the absorption band was much greater than for the $4f-4f$ transitions forbidden according to the Laporte rule.

The first studies on the Zeeman effect in Raman scattering were reported for the tervalent ytterbium ion in

yttrium gallium garnet. Here we shall consider the influence of this effect on the positions of the very intense electronic transitions of ytterbium aluminium garnet centred at 80 cm^{-1} (Fig. 13). The Zeeman spectrum of this Raman line is illustrated in Fig. 21, which shows that, for a zero magnetic field, cooling of the specimen from 77°K to 4.2°K alters the shape of the line. The intensity of the B transition at a frequency of 81.5 cm^{-1} decreases on the side of high energies. Since it has a higher energy than the A transition with a frequency of 74.6 cm^{-1}, one may reach certain conclusions concerning the energy level scheme; the relative positions of the levels are illustrated in Fig. 21. When a magnetic field is imposed, the distance between the two lower levels of the $^7F_6$ set of the TbAlG crystal field increases. The temperature of the crystal was 4.2°K, being immersed in liquid helium and the first excited state was unpopulated. Accordingly, the transition between levels with A (in group D_2) and B_3 or $B_2(D_2)$ symmetry disappears if the field and the distance between the levels increase. The single transition from the ground state shifts from 74.6 cm^{-1} to 79.5 cm^{-1} in a field of about 48 kG. In the crystal lattice unit cell of the garnet there are six sites for lanthanide ions, but the above experiments failed to reveal a fine structure. To some extent, this has also been observed for Dy^{3+} in garnets and one can now assume that the Zeeman Raman spectroscopic technique may be important, particularly in those cases where it is necessary to distinguish phonons and electronic transitions.

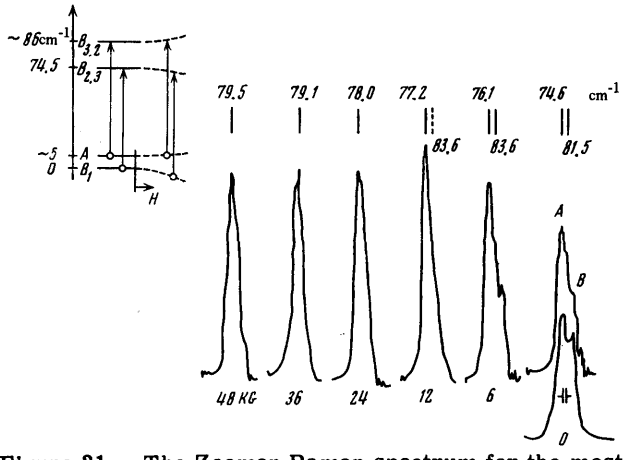


Figure 21. The Zeeman Raman spectrum for the most intense electronic effects in terbium aluminium garnet.

---o0o---

The present review deals exclusively with the interpretation and observation of light scattering at low electronic levels of lanthanide ions in solids. This type of light scattering is weaker than the usual scattering at vibrational levels but it has certain theoretical (and experimental) features which are not encountered in the usual Raman spectroscopy. All the experimental results presented are to some extent related to the effect of the crystal field on the lanthanide ion. It has been established that these results are particularly important for the elucidation of the nature of the crystal field in certain cubic crystals. Investigations of this kind have now been extended, particularly to the crystal field of transition metal ions in solids. Only limited information is available on this subject, but it appears that the main interest lies in the magnetic properties of transition metal compounds reflected in the characteristics of the scattering spectra.

REFERENCES

1. F. Rasetti, Z. Phys., 66, 646 (1930).
2. H. Gerding, Private communication.
3. J. Hougen and S. Singh, Phys. Rev. Letters, 10, 406 (1963).
4. R. J. Elliott and R. Loudon, Phys. Rev. Letters, 3, 189 (1963).
5. J. V. H. Chau, J. Chem. Phys., 44, 1708 (1966).
6. J. A. Koningstein, J. Opt. Soc. Amer., 56, 1405 (1966).
7. J. A. Koningstein, J. Chem. Phys., 46, 2811 (1967).
8. J. A. Koningstein and O. Sonnich-Mortensen, Phys. Rev. Letters, 18, 831 (1967).
9. J. A. Koningstein and O. Sonnich-Mortensen, Nature, 217, 445 (1968).
10. J. A. Koningstein and Tao-ning Ng, Canad. J. Chem., 47, B95 (1969).
11. J. A. Koningstein, Chem. Phys. Letters, 2, 238 (1968).
12. J. A. Koningstein and G. Schaack, Phys. Rev. B, [3], 2 (5), 1242 (1970).
13. J. D. Axe, Phys. Rev., 136, A42 (1964).
14. O. Sonnich-Mortensen and J. A. Koningstein, J. Chem. Phys., 48, 3971 (1968).
15. J. A. Koningstein and O. Sonnich-Mortensen, Phys. Rev., 168, 75 (1968).
16. J. A. Koningstein and O. Sonnich-Mortensen, Chem. Phys. Letters, 2, 693 (1968).
17. J. A. Koningstein and O. Sonnich-Mortensen, J. Opt. Soc. Amer., 58, 1208 (1968).
18. A. Kiel, T. Damen, S. P. S. Porto, S. Singh, and F. Varsanyi, Phys. Rev., 178, 1518 (1969).
19. J. A. Koningstein, Canad. J. Chem., 49, 2336 (1971).
20. R. L. Walsack, J. L. Lewis, B. E. Argyle, and R. K. Chang, Phys. Rev. B., [3], 3, 4342 (1971).
21. I. Dabrowski, P. Grunberg, and J. A. Koningstein, J. Chem. Phys., 56, 1264 (1972).
22. J. A. Koningstein, Phys. Rev., 174, 477 (1968).
23. J. Hougen and S. Singh, Proc. Roy. Soc., A277, 193 (1964).
24. G. Placzek, "Handbuch der Radiologie, Akademie Verlags. Leipzig, 1934, Vol. VI, Part II, p. 205.
25. A. C. Albrecht, J. Chem. Phys., 34, 1476 (1961).
26. E. B. Wilson, J. C. Decius, and P. C. Cross, "Molecular Vibrations", McGraw-Hill, New York, 1955.
27. C. W. Nielson and G. F. Koster, "Spectroscopic Coefficients for p^n, d^n, and f^n Configurations, M.I.T. Press, Cambridge, Massachusetts, 1963.
28. T. C. Damen, R. C. C. Leite, and S. P. S. Porto, Phys. Rev. Letters, 14, 9 (1965).
29. J. A. Köningstein and O. S. Mortensen, Chem. Phys. Letters, 1, 693 (1968).
30. A. Kiel and S. P. S. Porto, J. Mol. Spectroscopy, 32, 458 (1969).
31. G. Schaack and J. A. Koningstein, J. Opt. Soc. Amer., 60, 1110 (1970).

Faculty of Chemistry,
Carleton University,
Ottawa, Canada